Molecular Therapy
Methods & Clinical Development
Original Article

Adipose Mesenchymal Cells-Derived EVs Alleviate DOCA-Salt-Induced Hypertension by Promoting Cardio-Renal Protection

Rafael Soares Lindoso,[1,2,3] Jarlene Alécia Lopes,[1,2] Renata Binato,[4] Eliana Abdelhay,[4] Christina Maeda Takiya,[1] Kildare Rocha de Miranda,[1,2] Lucienne Silva Lara,[5] Antonella Viola,[6] Benedetta Bussolati,[7] Adalberto Vieyra,[1,2,3,8] and Federica Collino[1,3,6]

[1]Institute of Biophysics Carlos Chagas Filho, Federal University of Rio de Janeiro, 21941-902 Rio de Janeiro, Brazil; [2]National Center for Structural Biology and Bioimaging/CENABIO, Federal University of Rio de Janeiro, 21941-902 Rio de Janeiro, Brazil; [3]National Institute of Science and Technology for Regenerative Medicine-REGENERA, Federal University of Rio de Janeiro, 21941-902 Rio de Janeiro, Brazil; [4]Brazilian National Institute of Cancer, 20230-130 Rio de Janeiro, Brazil; [5]Institute of Biomedical Sciences, Federal University of Rio de Janeiro, 21941-590 Rio de Janeiro, Brazil; [6]Department of Biomedical Sciences and Pediatric Research Institute "Citta della Speranza," University of Padova, 35131 Padua, Italy; [7]Department of Molecular Biotechnology and Health Sciences, University of Torino, 10126 Turin, Italy; [8]Graduate Program of Translational Biomedicine/BIOTRANS, Grande Rio University, 25071-202 Duque de Caxias, Brazil

Hypertension is a long-term condition that can increase organ susceptibility to insults and lead to severe complications such as chronic kidney disease (CKD). Extracellular vesicles (EVs) are cell-derived membrane structures that participate in cell-cell communication by exporting encapsulated molecules to target cells, regulating physiological and pathological processes. We here demonstrate that multiple administration of EVs from adipose-derived mesenchymal stromal cells (ASC-EVs) in deoxycorticosterone acetate (DOCA)-salt hypertensive model can protect renal tissue by maintaining its filtration capacity. Indeed, ASC-EVs downregulated the pro-inflammatory molecules monocyte chemoattracting protein-1 (MCP-1) and plasminogen activating inhibitor-1 (PAI1) and reduced recruitment of macrophages in the kidney. Moreover, ASC-EVs prevented cardiac tissue fibrosis and maintained blood pressure within normal levels, thus demonstrating their multiple favorable effects in different organs. By applying microRNA (miRNA) microarray profile of the kidney of DOCA-salt rats, we identified a selective miRNA signature associated with epithelial-mesenchymal transition (EMT). One of the key pathways found was the axis miR-200-TGF-β, that was significantly altered by EV administration, thereby affecting the EMT signaling and preventing renal inflammatory response and fibrosis development. Our results indicate that EVs can be a potent therapeutic tool for the treatment of hypertension-induced CKD in cardio-renal syndrome.

INTRODUCTION

Hypertension (HTN) is a complex multifactorial disease that results in raised blood pressure and represents a comorbidity factor for the development of cardiovascular and kidney diseases.[1–3]

In the kidney, long-term HTN can lead to the increase of intraglomerular pressure, glomerular damage, and impairment of the filtration process. As a consequence, adaptive changes in nephrons occur to compensate the initial damage, possibly leading to profibrotic maladaptive modifications, loss of nephrons, and, consequently, to a faster decline in the kidney functions.[4] Moreover, the fibrotic process is associated with the release of inflammatory mediators and recruitment of inflammatory/immune cells that contribute to chronic kidney disease (CKD).[5] Although the kidney has an intrinsic regenerative capacity, chronic conditions limit its ability to recover from insults.[6]

Regarding the cardiovascular system, progressive HTN drastically induces cardiac changes that include cardiac hypertrophy and fibrosis, ultimately causing myocardial stiffening and expansion, together with deterioration of the heart electrical conduction and vascular hypertrophy and dysfunction.[7] Moreover, in hypertensive patients the development of cardiac damage has been associated with the overactivity of the renin-angiotensin-aldosterone system.[8]

In addition to causing direct cardiac and renal injury, HTN also predisposes patients to the so-called "cardio-renal syndrome" (CRS), which refers to various conditions where dysfunction of either the heart or kidneys leads to dysfunction of the other organs.[9–11] Although its pathogenesis is not fully understood, several experimental models have been developed to investigate the multiple factors associated with CRS.[12]

Received 10 September 2019; accepted 2 November 2019;
https://doi.org/10.1016/j.omtm.2019.11.002.

Correspondence: Federica Collino, PhD, Department of Biomedical Sciences and Pediatric Research Institute "Citta della Speranza, University of Padova, 35131 Padua, Italy.
E-mail: federica.collino@unipd.it
Correspondence: Adalberto Vieyra, MD, Institute of Biophysics Carlos Chagas Filho, Federal University of Rio de Janeiro, 21941-902, Rio de Janeiro, Brazil.
E-mail: adalberto.vieyra@biof.ufrj.br

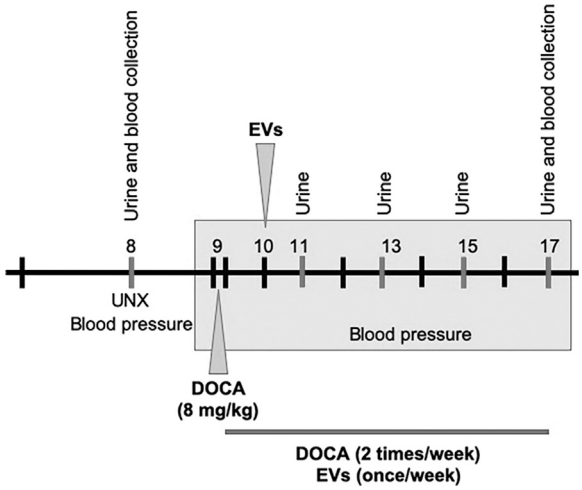

Figure 1. Schematic Representation of the Time Course of the Experimental Protocol

Rats were subjected to unilateral nephrectomy (left kidney) at the age of 8 weeks (first vertical line), and after 1 week were divided in the following experimental groups: (1) uninephrectomized rats with standard-salt diet chow (UNX, n = 10); (2) UNX with high Na^+ diet plus DOCA twice a week (DOCA, n = 16); UNX with high salt plus DOCA injected i.v. weekly with EVs (DOCA-EV, n = 10). Animals were monitored weekly for systolic blood pressure (SBP). For the sake of clarity, only the first administration of DOCA and EVs are indicated. Urine samples were collected every 2 weeks (vertical lines indicated as Urine) from weeks 9–17, and terminal blood pressure, urine, and blood collection were finally performed at the time of sacrifice (last vertical line). A 4th group of Sham (false operated) rats that received standard-salt diet was also analyzed (SHAM, n = 8).

The deoxycorticosterone acetate (DOCA)-salt model provides an imbalance of renal Na^+ handling due to the administration of the aldosterone precursor DOCA, which increases Na^+ and water reabsorption by the distal nephron, promoting hypervolemia and consequently inducing hypertension.[13] Administration of a high-salt diet in combination with uninephrectomy also drastically increases the onset of hypertension.[13] An overactive sympathetic nervous system seems to have a central role in the development of hypertension in DOCA-salt rats, raising blood pressure through its direct effect on venous smooth muscle tone and peripheral vascular resistance.[14] As a result, DOCA-salt treated animals provide a chronic vascular remodeling, with development of hypertrophy, fibrosis, and inflammatory cell infiltration in the heart and the kidney,[15,16] along with activation of renal transforming growth factor β (TGF-β) expression.[17]

The potential benefit of mesenchymal stromal cells (MSCs) in the treatment of kidney diseases has been widely studied.[18] Among the different sources of MSCs, adipose tissue is an easy and repeatable harvested source. Adipose-derived mesenchymal cells (ASCs) have immunosuppressive properties, low immunogenicity and secrete trophic factors that support tissue regeneration.[19]

The main mechanism of action of bone marrow and tissue MSCs has been attributed to the secretion of extracellular vesicles (EVs), membrane structures that carry bioactive molecules (proteins, lipids, and nucleic acids) regulating different cellular processes in the recipient cells.[20] The beneficial effects of MSC-EVs in different pathological states are associated with reduction of inflammatory infiltrate and decrease of fibrosis, which represent important processes also in CKD pathophysiology.[21] An important role of MSC has been shown in EVs by limiting acute to chronic kidney injury transition and progression.[22–24]

We have tested the hypothesis that ASC derived EVs (ASC-EVs) can positively modulate the development of CKD by affecting inflammation and fibrosis in the cardio-renal system in DOCA-salt treated rats. In view of the importance of microRNA (miRNAs) in these processes, we have also evaluated the possible involvement of a specific kidney miRNAs signature in DOCA-salt induced CRS and the impact of EVs on these pathways.

RESULTS

Characterization of ASC-EVs

ASCs cultured for 72 h in EVs collection medium were analyzed by transmission electron microscopy (TEM) (Figure S1A). Vesicular structures of different size were detected on the surface of the cells, indicating the existence of active release of EVs from ASCs (Figure S1A). EVs were collected from ASCs as described in the Materials and Methods and their presence was confirmed by TEM (Figure S1B). EVs are heterogeneous in size and comprise small and large size vesicle populations. Nanoparticle tracking analysis (NTA) was used to characterize and count EVs, which in this case was a heterogeneous pattern (Figure S1C), with a mean size distribution of 114.1 ± 8.6 nm and a mean value of 5,752 ± 487 particles released for each cell (EV preparations, n = 10). Flow cytometry analysis showed the expression by ASC-EVs of the exosome markers CD63 and CD81, but not CD9 (Figure S1D).

ASC-EV Treatment Prevent the Progressive Increase of Blood Pressure in DOCA-Salt Rats

We evaluated the effect of ASC-EV administration in the hypertensive rat model DOCA-salt (Figure 1). With respect of UNX rats, the DOCA animals (treated with DOCA-salt) lost significant body weight (Figure 2A) after 8 weeks from the unilateral nephrectomy ($p < 0.05$). The nephrectomy procedure (UNX) did not affect body weight as detected by the comparison with control Sham rats (SHAM, Figure 2A).

Systolic blood pressure (SBP) was recorded before and 1 week after uninephrectomy; no modification was observed in rats submitted to the surgical procedure (133.6 ± 2.7 versus 135.3 ± 4.0 mmHg, before and after nephrectomy, respectively). The SBP was measured every week for 8 weeks and a steadily increase in DOCA animals was recorded during the entire treatment period (Figure 2B). By week 4, SBP was significantly elevated in DOCA-salt animals compared to UNX and SHAM rats ($p < 0.05$ versus control animals). However, weekly injections of EVs from week 2 after nephrectomy in DOCA rats (DOCA-EV), were able to alleviate any further increase in SBP induced by DOCA-salt treatment from week 5 from nephrectomy. This pressure profile was maintained until sacrifice, indicating that EV treatment could mitigate the increase in DOCA-salt induced SBP. At week 9, the DOCA group had the highest SBP and diastolic blood pressure (DBP), which

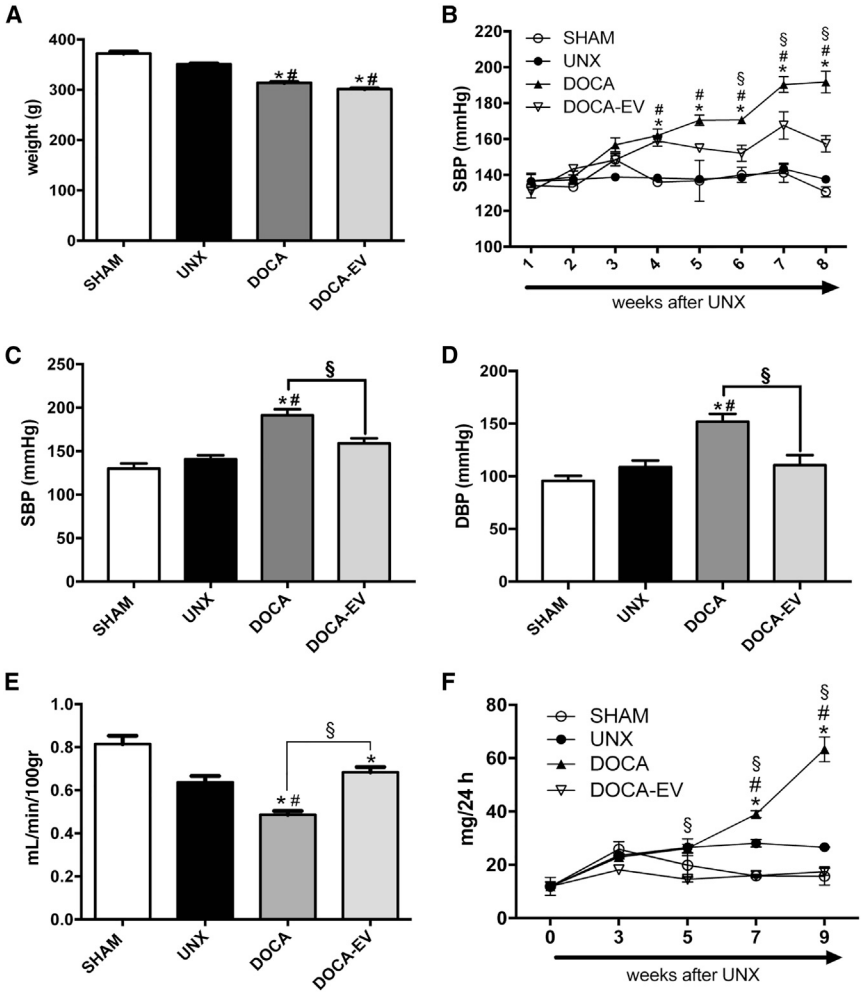

Figure 2. ASC-EVs Normalized Hypertension and Prevented CKD Progression in DOCA-Salt Rats

(A) Body weight was measured in DOCA-salt treated rats at time of sacrifice (week 9) and compared with untreated UNX animals (UNX, n = 9; DOCA, n = 13; DOCA-EV, n = 10). A group of false operated animals was also analyzed (SHAM, n = 8). (B) SBP of DOCA rats were recorded every week after nephrectomy (UNX) for 8 weeks (1–8 weeks) and compared with untreated UNX animals and SHAM animals. The value of SBP reported is the mean of blood pressure of all the animals tested in each experimental group at each time point (SHAM, n = 4; UNX, n = 9; DOCA, n = 13; DOCA-EV, n = 10). SBP (C) and diastolic blood pressure (DBP) (D) were recorded before sacrifice (week 9) for all the animals tested in the 4 experimental groups (number of animals, n = 8–13). (E) Measure of creatinine clearance (CrC) normalized for body weight and expressed as mL/min/100 g measured for all the animals tested in the 4 experimental groups (number of animals, n = 8–13). (F) Time course of 24 h-protein urinary excretion (mg/24 h) before nephrectomy until sacrifice (SHAM, n = 4; UNX, n = 9; DOCA, n = 13; DOCA-EV, n = 10). All data represent mean ± SE. *indicates statistical difference to SHAM group; # indicates statistical difference to UNX group, § indicates statistical difference to DOCA-EV group; $p < 0.05$.

were indeed reduced in EV-treated DOCA animals (Figures 2C and 2D). EV treatment did not affect reduction of body weight induced by DOCA-salt at time of sacrifice (Figure 2A).

ASC-EVs Improved Renal Function Parameters and Decreased Urinary Protein Excretion in DOCA-Salt Rats

Time-course analysis of 24 h-water consumption indicated a significant increase in this parameter in DOCA animals at week 3 after nephrectomy with respect to SHAM and UNX animals (110.6 ± 1.3, 28.4 ± 0.2, and 44.83 ± 1.5, respectively, $p < 0.05$ in respect to controls). The same was observed for the urinary volume (12.7 ± 0.1, 3.3 ± 0.3, and 3.5 ± 0.2, respectively, $p < 0.05$ in respect to controls). EV treatment transiently ameliorated the polyuria state of DOCA rats as measured by the urinary volume at weeks 3 (DOCA-EV, 10.3 ± 0.4, $p < 0.05$ in respect to DOCA) and 5 (DOCA, 10.68 ± 0.1 and DOCA-EV, 8.33 ± 0.1, $p < 0.05$ in respect to DOCA) but it had no effect at later time points (data not shown). As illustrated in Table S1, together with the 24 h-urinary volume, Na^+ excretion at week 9 was significantly increased in DOCA rats compared to SHAM and UNX animals, which was not modified by the EV treatment. All the 3 treated groups showed a significant reduction in K^+ excretion compared to SHAM rats, with no difference between them (Table S1).

The impact of increased systemic HTN on renal function was subsequently investigated, including proteinuria development and the effect of EV administration. There was a significant increase in plasma creatinine levels (Table S1) together with a significant reduction in the creatinine clearance in DOCA rats with respect to UNX (30%) and SHAM animals (~50%) (Figure 2E). EV treatment restored normal plasma creatinine levels and a creatinine clearance similar to the UNX rats. In parallel, hypertensive DOCA animals developed progressive proteinuria compared to SHAM and UNX animals, reaching a significant increase at week 9, measured by 24 h protein excretion levels (Figure 2F) and as the urinary protein/creatinine ratio (UP:Cr; Table S1). As for functional parameters, ASC-EV treatment significantly reduced 24 h protein excretion (Figure 2F) and the UP:Cr ratio (Table S1) in DOCA salt-treated animals, supporting the view that EVs actively protect against kidney damage. Hypertensive rats also developed albuminuria, which was expressed as the urinary albumin/creatinine ratio (UA:Cr, Table S1). ASC-EV treatment significantly decreased albuminuria in DOCA animals (Table S1).

ASC-EVs Improved Morphology and Reduced Classical Markers of Kidney Damage in DOCA-Salt Rats

Besides the examination of biochemical parameters, renal damage was then quantified with respect to renal hypertrophy and by

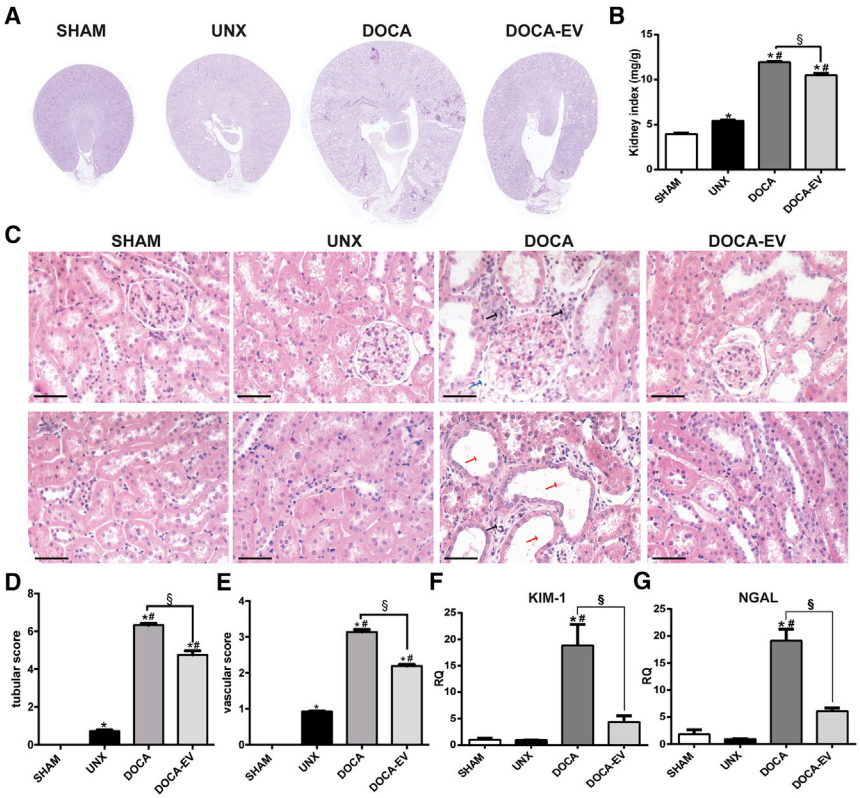

Figure 3. ASC-EV Treatment Improved Morphology and Reduced Classical Markers of Kidney Damage in DOCA-Salt Rats

(A) Representative image of a transverse section of the entire kidney stained with H&E of 9-week-treated rats under different experimental conditions, as indicated at the top of the panels. (B) Right kidney weight normalized by the body weight (mg/g) of 9-week-treated rats measured for all the animals tested in the 4 experimental groups (SHAM, n = 4; UNX, n = 9; DOCA, n = 13; DOCA-EV, n = 10). (C) Representative photomicrographs of the kidney cortex showing glomerular (upper images) and tubular structures (lower images) in kidney sections from the 4 groups, as indicated in the top of the panels. H&E was used as staining (scale bars, 50 μm). Black arrows indicate inflammatory cells infiltration; red arrows indicate tubular dilation; blue arrows indicate extracellular matrix expansion and glomerulosclerosis. (D and E) Histological score of tubular (D) and vascular (E) lesions of the kidneys of all the animals tested in the 4 experimental groups (SHAM, n = 4; UNX, n = 9; DOCA, n = 13; DOCA-EV, n = 10), quantified as described in the Materials and Methods section. (F and G) *KIM-1* (F) and *NGAL* (G) mRNA levels in the renal tissue of SHAM (n = 3) and in the uninephrectomized groups (UNX, n = 6; DOCA and DOCA-EV, n = 7). Quantitative real-time PCR data were expressed as relative quantification (RQ) and UNX was used as the reference sample. Data represent mean ± SE. *indicates statistical difference to SHAM group, # indicates statistical difference to UNX group, and § indicates statistical difference to DOCA-EV group; $p < 0.05$.

histological analysis. Figure 3A shows that kidneys had accentuated hypertrophy provoked by DOCA-salt treatment, which was ameliorated by EV administration. There was also a significant difference in the kidney-to-body weight ratio between DOCA and both SHAM and UNX rats (11.9 ± 0.07 versus 4.0 ± 0.09 and 5.4 ± 0.08, respectively; Figure 3B). ASC-EV treatment resulted in a modest (20%), but significant, reduction in the kidney-to-body weight compared with DOCA ($p < 0.05$). H&E staining showed increased tubular damage (including atrophy, loss of brush border, and presence of protein casts), along with an accumulation of interstitial matrix and evidence of inflammation in the cortex of DOCA rats compared to SHAM and UNX controls (Figure 3C), which were ameliorated in EVs-treated rats.

The quantitative measure of tubular damage was higher in DOCA rats (6.3 ± 0.33) with very slight injury in the UNX group (0.7 ± 0.21; Figure 3D). DOCA rats also developed vascular damage (3.1 ± 0.07), which was very low in the UNX group (0.9 ± 0.01), with no such signs being seen in SHAM animals (Figure 3E). DOCA-EV rats showed significantly less tubular and vascular damage (4.7 ± 0.69 and 2.2 ± 0.04, $p < 0.05$ compared to DOCA). The degree of injury was confirmed by measuring expression of 2 markers of kidney injury, namely kidney injury molecule-1 (KIM-1) and neutrophil gelatinase-associated lipocalin (NGAL) (Figures 3F and 3G). Compared to the other experimental groups, the DOCA animals expressed 20-fold higher levels of *KIM-1* and *NGAL* ($p < 0.05$) in the kidney, but EV treatment significantly reduced these values (Figures 3F and 3G).

To measure the presence of proliferating cells, we used immunohistochemistry for proliferating cell nuclear antigen (PCNA) (Figure S2A). PCNA-positive cells occurred in DOCA rats, in the interstitial tissue and in the tubules, both in the cortical region (excluding glomeruli) and inner medulla (Figure S2A). Also in this case, EV treatment markedly attenuated (~50%) cell proliferation in the cortical and medullary areas of the kidney (Figure S2B).

The effects of DOCA-salt treatment on apoptosis were also examined by determining the ratio of pro-apoptotic protein Bax to the anti-apoptotic protein Bcl-2 (Figure S2C). The Bax/Bcl-2 protein ratio increased 100% in the kidneys of DOCA rats compared with UNX animals, whereas the EV treatment reversed the ratio to the levels of the control rats.

ASC-EVs Attenuated Renal Fibrosis in Rats Induced by DOCA-Salt Treatment

Analysis of renal fibrosis by Picrosirius red staining indicated the presence of collagen deposition in the kidneys of hypertensive rats, primarily in the interstitial space (Figure 4A). Figure 4B shows kidney immunostaining of alpha-smooth muscle actin (α-SMA), a marker of myofibroblasts. In SHAM and UNX rats, positive physiological

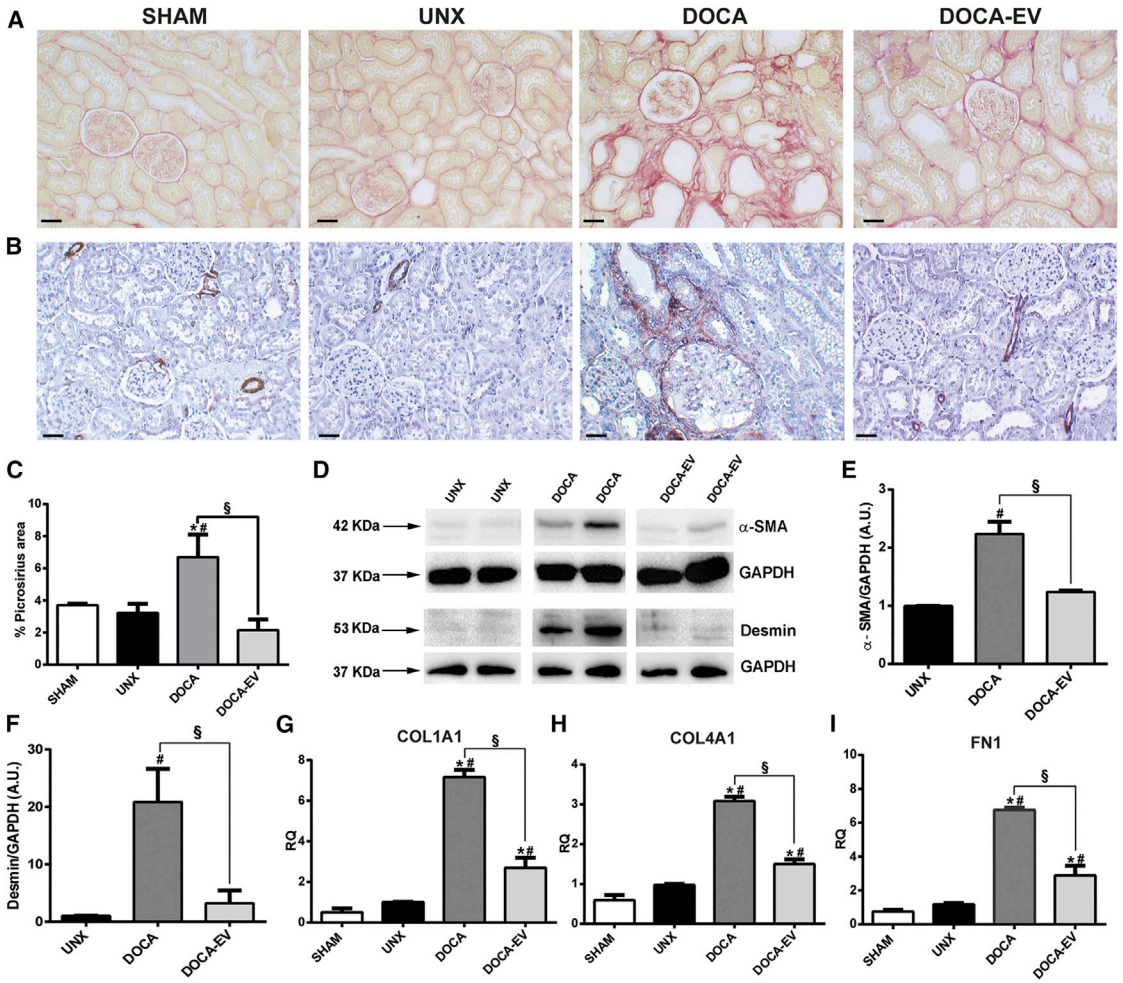

Figure 4. ASC-EV Treatment Promoted Important Attenuation of Kidney Fibrosis in the DOCA-Salt Model

(A) Representative photomicrographs of kidney slices stained with Picrosirius red on 9-week-treated rats from the 4 experimental groups (scale bars, 50 μm). (B) α-SMA expression in the kidney of 9-week-treated rats under the different experimental conditions was determined by immunohistochemistry (n = 4 for each treatment) (scale bars, 50 μm). (C) Quantification of Picrosirius red stained area in kidney sections expressed as a percentage of the total area of the kidney, in 9-week-treated rats, measured for all the animals tested in the 4 experimental groups (SHAM, n = 4; UNX, n = 9; DOCA, n = 13; DOCA-EV, n = 10). (D–F) Western blot analysis of α-SMA and Desmin in the cortex of 9-week-treated UNX (n = 6), DOCA, and DOCA-EV (n = 8) rats. GAPDH was used as loading control. Values represent the fold increase with respect to UNX (considered as the reference = 1). (G–I) Analysis of *COL1A1*, *COL4A1*, and *FN* mRNA levels in the renal tissue in control SHAM (n = 3) and in all the uninephrectomized animal groups (UNX, n = 6; DOCA and DOCA-EV, n = 7). qRT-PCR data were expressed as RQ and UNX was used as the reference sample. Data represent mean ± SE. *indicates statistical difference to SHAM group, # indicates statistical difference to UNX group, and § indicates statistical difference to DOCA group; $p < 0.05$.

staining of α-SMA was found only in the blood vessels (Figure 4B), whereas α-SMA was localized in the interstitial and periglomerular regions in DOCA rats. Quantification of the Picrosirius red staining demonstrated an increase in collagen deposition by 100% in the kidneys of DOCA rats, that was absent in DOCA-salt rats treated with ASC-EVs (Figure 4C). Moreover, α-SMA expression was significantly increased in the kidney of DOCA rats compared to the UNX, as detected by western blotting analysis (Figures 4D and 4E). EV treatment of DOCA rats reduced expression of α-SMA (Figures 4D and 4E), which had localized similarly to that seen in UNX rats (Figure 4B). We also detected a significant increase in the glomerular damage marker, Desmin, in DOCA rats, which was almost absent in UNX and DOCA-EV animals (Figures 4D and 4F). Glomerular lesions were detected in DOCA animals by quantitative measure of the glomerular damage score (1.7 ± 0.03, for DOCA), which was significantly reduced in both the UNX and DOCA-EV groups (0.9 ± 0.01 and 1.3 ± 0.07, $p < 0.05$). These structural improvements induced by the EV treatment were accompanied by a decrease in the gene expression of profibrotic collagens (*Col1A1*, *Col4A1*) and fibronectin (*FN1*) genes (Figures 4G–4I).

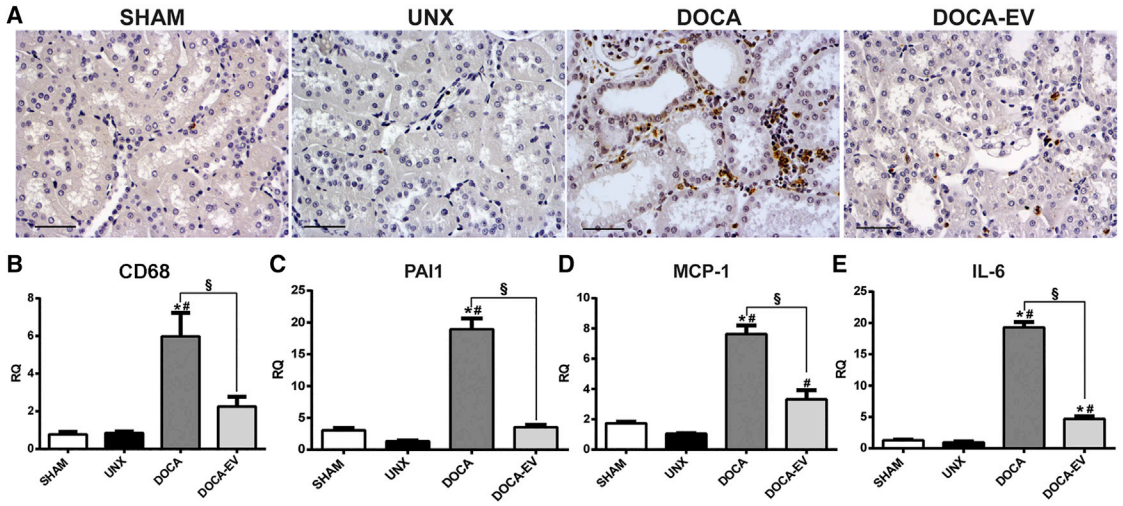

Figure 5. ASC-EVs Have Accentuated Anti-Inflammatory Properties in the DOCA-Salt Model

(A) Representative photomicrograph of ECD68 macrophage cell-surface marker expression determined by immunohistochemistry in the kidneys of 9-week-treated rats under the experimental conditions indicated at the top of the panels (scale bars, 50 μm). (B–E) Analysis of *CD68* (B), *PAI1* (C), *MCP-1* (D), and *IL-6* (E) mRNA levels in the renal tissue in control SHAM (n = 3) and in all the uninephrectomized animals (UNX, n = 6; DOCA and DOCA-EV, n = 7). qRT-PCR data were expressed as RQ and UNX was used as reference sample. Data represent mean ± SE. *indicates statistical difference to SHAM group, # indicates statistical difference to UNX group, and § indicates statistical difference to DOCA-EV group; $p < 0.05$.

ASC-EVs Reduced the Expression of Pro-Inflammatory Cytokines and Macrophage Infiltration of the Kidney

Immunohistochemical staining of cluster of differentiation 68 (CD68), a specific macrophage cell-surface marker, showed massive macrophage infiltration in response to DOCA-salt treatment (Figure 5A). The increased accumulation of CD68 in the renal interstitial space of DOCA rats was also quantitatively confirmed at the mRNA level by 6-fold, showing that EV treatment reduced gene expression of *CD68* to levels that were no different from that of control animals (Figure 5B). In DOCA rats, EVs were also effective in reducing the mRNA expression of the plasminogen activator inhibitor-1 (*PAI1*) and the inflammatory molecules monocyte chemoattracting-1 (*MCP-1*) and interleukin-6 (*IL-6*) (Figure 5C–5E).

ASC-EVs Attenuated Cardiac Fibrosis in Rats Induced by DOCA-Salt Treatment

As in the case of the kidney, cardiac fibrosis was drastically increased in DOCA rats, with accumulation of interstitial and perivascular collagen, as determined by Masson's trichrome (Figure 6A) and Picrosirius red staining (Figure 6B). An increase of cardiac fibrosis was associated with inflammation in the heart, detected by the presence of foci of CD68-positive macrophages in DOCA rats (Figure 6C). Fibrosis and infiltrating macrophages were significantly attenuated by treatment with EVs, confirmed by quantitative analyses (Figures 6D and 6E). Hypertensive DOCA-treated rats had cardiac hypertrophy, which was absent in the normotensive SHAM and UNX animals, measured by the heart index (heart weight/body weight ratio; DOCA, 4.8 ± 0.02; SHAM, 3.6 ± 0.04; and UNX, 3.3 ± 0.01, respectively). In this case, the EV treatment also lowered the heart-to-body weight ratio in DOCA rats (4.4 ± 0.02, $p < 0.05$), but it remained higher than controls (Figure 6F).

DOCA-Salt Treatment Modulates miRNA Expression in the Renal Lesions

To test the hypothesis that renal fibrosis and inflammation in DOCA-salt can be associated with a distinctive miRNA signature, we screened renal samples from SHAM, UNX, DOCA, and DOCA-EV rats for the expression of 758 mature rodent miRNAs. A total of 553 miRNAs were detected in at least 3 of 4 renal samples (80%) analyzed among the entire mature rodent miRNA panel. Hierarchical clustering analysis of all the groups highlighted the generation of 5 different clusters of expression (Figure 7A). Moreover, fold-change analysis indicated that 149 miRNAs were differentially expressed between DOCA rats and all the other 3 experimental groups (Table S2).

EV treatment induced modification of the miRNA signature in DOCA-salt treated rats, with 56 miRNAs being upregulated (Figure 7B, upper part) and 19 downregulated (Figure 7B, lower part) in DOCA-EV with respect to DOCA rat kidneys. Of interest, 36 upregulated and 14 downregulated miRNAs in DOCA-EV were commonly found in UNX-treated rats only, highlighting that, after EV treatment, the miRNA signature of DOCA-salt rats was restored toward the changes found in nephrectomized rats that had no signs of renal injury.

Aiming to define the differential molecular signature between DOCA and the groups UNX and DOCA-EV, we conducted *in silico* analysis of the differentially expressed miRNAs. Starting from input miRNAs,

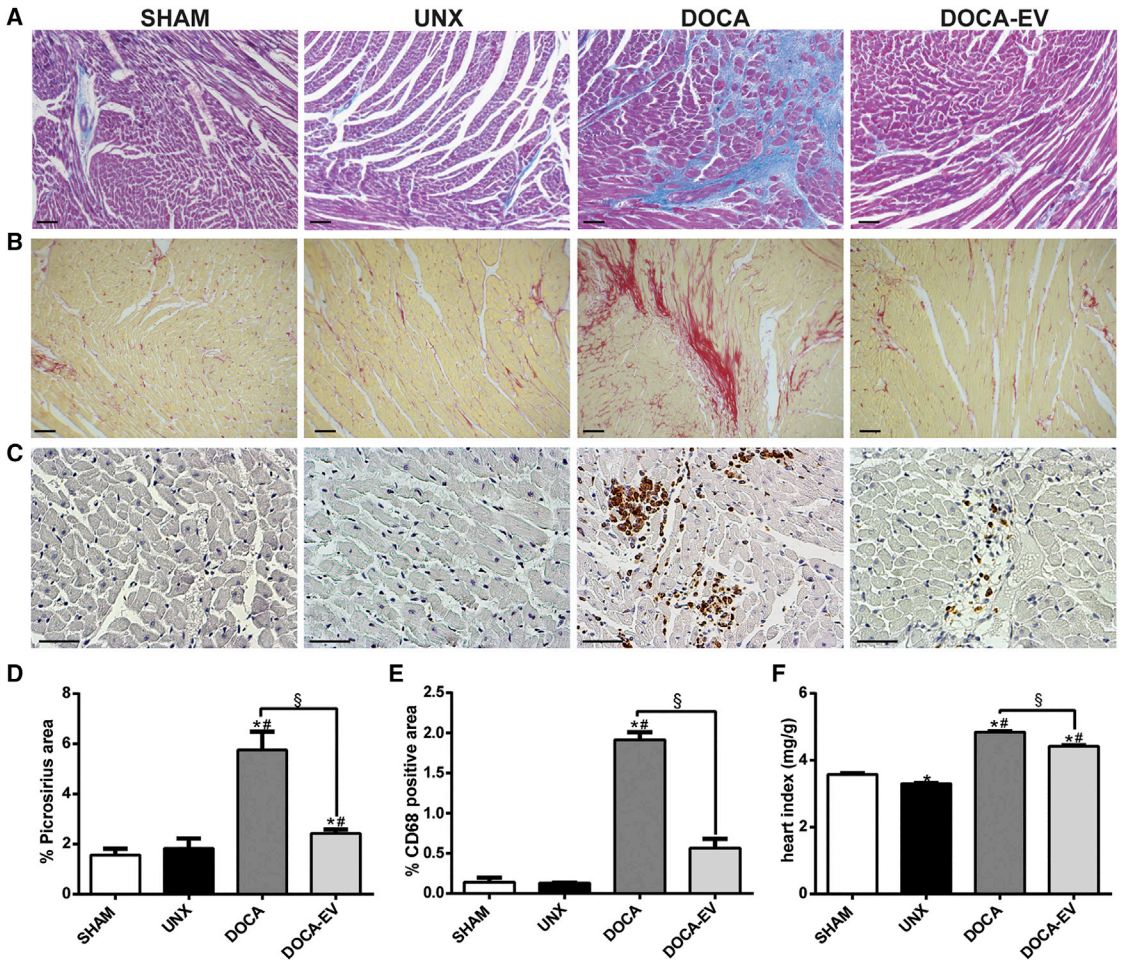

Figure 6. ASC-EVs Markedly Attenuated Cardiac Fibrosis Induced in Rats by DOCA-Salt Treatment

(A and B) Representative photomicrographs of heart slices stained with Masson's trichrome and Picrosirius red of 9-week-treated rats of the different experimental groups indicated at the top (scale bars, 50 μm). (C) Representative photomicrograph of CD68 marker expression determined by immunohistochemistry in the heart of 9-week-treated rats under the different experimental conditions (scale bars, 50 μm). (D) Quantification of Picrosirius red staining area expressed as a percentage of total area of the heart in 9-week-treated rats measured for all the animals in the 4 experimental groups (SHAM, n = 4; UNX, n = 9; DOCA, n = 13; DOCA-EV, n = 10). (E) Quantification of CD68-positive area expressed as a percentage of positive area/field (10 fields/animal), determined by immunohistochemistry in the heart of 9-week-treated rats (n = 4 animals for each treatment). (F) Heart weights with respect to body weight (mg/g) of 9-week-treated rats of each experimental group measured for all the animals tested in the 4 experimental groups (SHAM, n = 4; UNX, n = 9; DOCA, n = 13; DOCA-EV, n = 10). Data represent mean ± SE. *indicates statistical difference to SHAM group, # indicates statistical difference to UNX group, and § indicates statistical difference to DOCA group; $p < 0.05$.

it was possible to identify predicted and validated target genes and categorize them to produce representative pathway maps.[25] The processes associated with these genes are related to cellular response to amino acids and chemical stimulus, including a wide ensemble of cellular responses to different oxygen- and nitrogen-containing compounds (Figure 7C).

Interestingly, the most representative network of the common differentially expressed miRNAs was associated with the development and regulation of epithelial-mesenchymal transition (EMT; Figure 8A). The miR-200 family members and their direct target nodes were highlighted as overrepresented elements involved in DOCA-salt treatment (Figure 8A). To validate these data, we further analyzed miR-200a-3p, -200b-3p, -200c-3p, -141 and -429 in the kidneys by quantitative real-time PCR; their expression levels were significantly lower in the DOCA groups than those in the controls (SHAM and UNX). EV treatment reversed the DOCA-salt regulation in all the miR-200 family investigated, also upregulating miR-200c-3p, which was unmodified in DOCA and control samples (Figure 8B).

ASC-EVs Downregulated Profibrotic Genes in DOCA-Salt Treated Rats

Direct nodes of the miR-200 family were the zinc finger E-box binding homeobox 1 (*ZEB1*) and 2 (*ZEB2*), also known as *TCF8* and *SIP1*, respectively. Expression of *TCF8* and *SIP1* was significantly elevated in DOCA-salt treated animals with respect to SHAM (Figures 8C

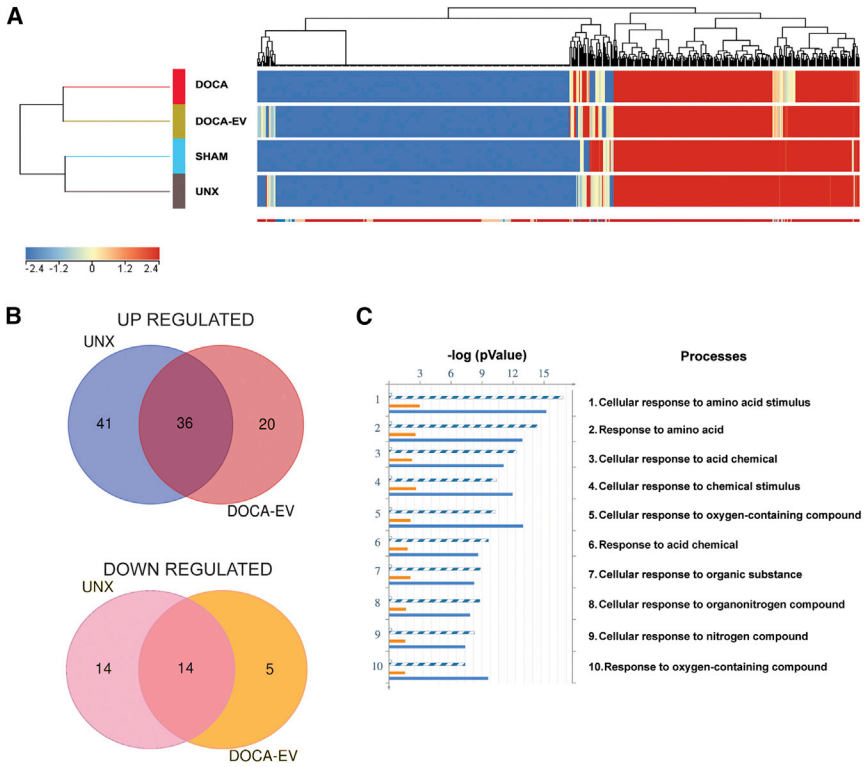

Figure 7. A Healing miRNA Signature Was Generated by ASC-EV Administration

(A) Hierarchical clustering analysis of the 553 rat miRNAs expressed in the kidney of 9-week-treated rats under the different experimental conditions (SHAM, UNX, DOCA, and DOCA-EV groups, n = 2 for each condition from 4 animals/group). (B) Venn diagrams of the upregulated (upper panel) and downregulated (lower panel) miRNAs in the kidneys of the UNX and DOCA-EV groups with respect to DOCA. The diagrams show the commonly or selectively modulated miRNAs. (C) Significantly enriched biological processes associated with the identified target genes of the differentially expressed miRNAs in DOCA animals with respect to UNX or DOCA-EV, indicated by the marks/colors of the horizontal bars (blue and white, common miRNAs; red, DOCA-EV selective; blue, UNX selective).

and 8D). EV treatment reduced the upregulation of these genes after DOCA-salt treatment to the levels of UNX renal specimens (Figures 8C and 8D; $p < 0.05$). Other pro-fibrotic genes directly or indirectly connected with the miR-200 family and involved in EMT, such as connective tissue growth factor (*CTGF*), *TGF-β1*, and *TGF-β2*, were then tested. DOCA-salt treatment induced a strong upregulation of all these EMT genes, whereas EV administration had the opposite effect (Figures 7E–7G). The zinc-finger-containing transcription factors Slug 1 and 2 (*SNAI1* and *SNAI2*) are known to repress transcription of E-cadherin and stimulate vascular endothelial cadherin and fibronectin genes.[26] Quantitative real-time PCR showed a stimulatory effect of DOCA-salt treatment on *SNAI1* and *SNAI2* mRNA, which was totally blocked by EV treatment (Figures 8H and 8I). Together with the enhancement of *TGF-β1* expression, the DOCA-salt treatment also induced upregulation of miR-155-5p, an important miRNA associated with EMT; again, upregulation of miR-155-5p was abrogated by EVs (Figure 8J).

DISCUSSION

We here demonstrate that multiple administration of ASC-EVs in a hypertensive-induced CKD model promotes protection from renal damage, conservation of renal function, reduction of the inflammatory response, and prevention of interstitial fibrosis in the kidney. ASC-EVs also prevented fibrosis in cardiac tissue and maintained the blood pressure within normal levels, displaying complex and multiorgan beneficial effects in the complex pathophysiology of DOCA-salt-induced CRS. We also identified a distinctive EMT miRNA signature induced by DOCA treatment that directly correlated with increased TGF-β gene expression and renal damage. All of these molecular modifications were reversed by ASC-EV administration. Renal damage and TGF-β upregulation are also associated in diseases, such as diabetes.[27]

CKD is characterized by several structural changes in the kidney that result in a progressive loss of nephrons and renal function.[28] The DOCA-salt model mimics a multifactorial pathological state associated with CKD. Although it presents some limitations to represent the entire complexity of chronic disease, the model encloses several aspects, including the increase in blood pressure, kidney and heart hypertrophy, renal tubular and vascular damage, and extensive development of fibrosis.

Different studies reported the engagement of several primary mechanisms of hormonal, renal, and neural origin as a requirement for the raising of blood pressure observed in this model.[29] In the kidney, the retention of Na^+, and subsequently of water, as an attempt to maintain plasma osmolality, distinctly participates in DOCA-salt hypertension.[30,31] Moreover, the high Na^+ diet load for 8 weeks together with injection of DOCA, results in severe HTN, strongly interconnected with renal function deterioration and glomerular damage, as indicated by the development of proteinuria and reduction of the creatinine clearance.[32] We also observed that long-term induced HTN causes tubular injury and microvasculature rarefaction, inducing renal damage in DOCA-salt rats. This was accompanied by a strong induction of pro-oxidative processes associated with the upregulation of the pro-apoptotic protein, Bax, and the downregulation of the anti-apoptotic protein, Bcl-2—a prelude to cell death.[33]

Previous observations demonstrated the anti-fibrotic effects of EVs derived from different MSC types (bone-marrow derived, adipose-tissue derived, and liver derived) in different CKD models.[34–36] Our analyses for the first time show the effect of ASC-EV treatment in a

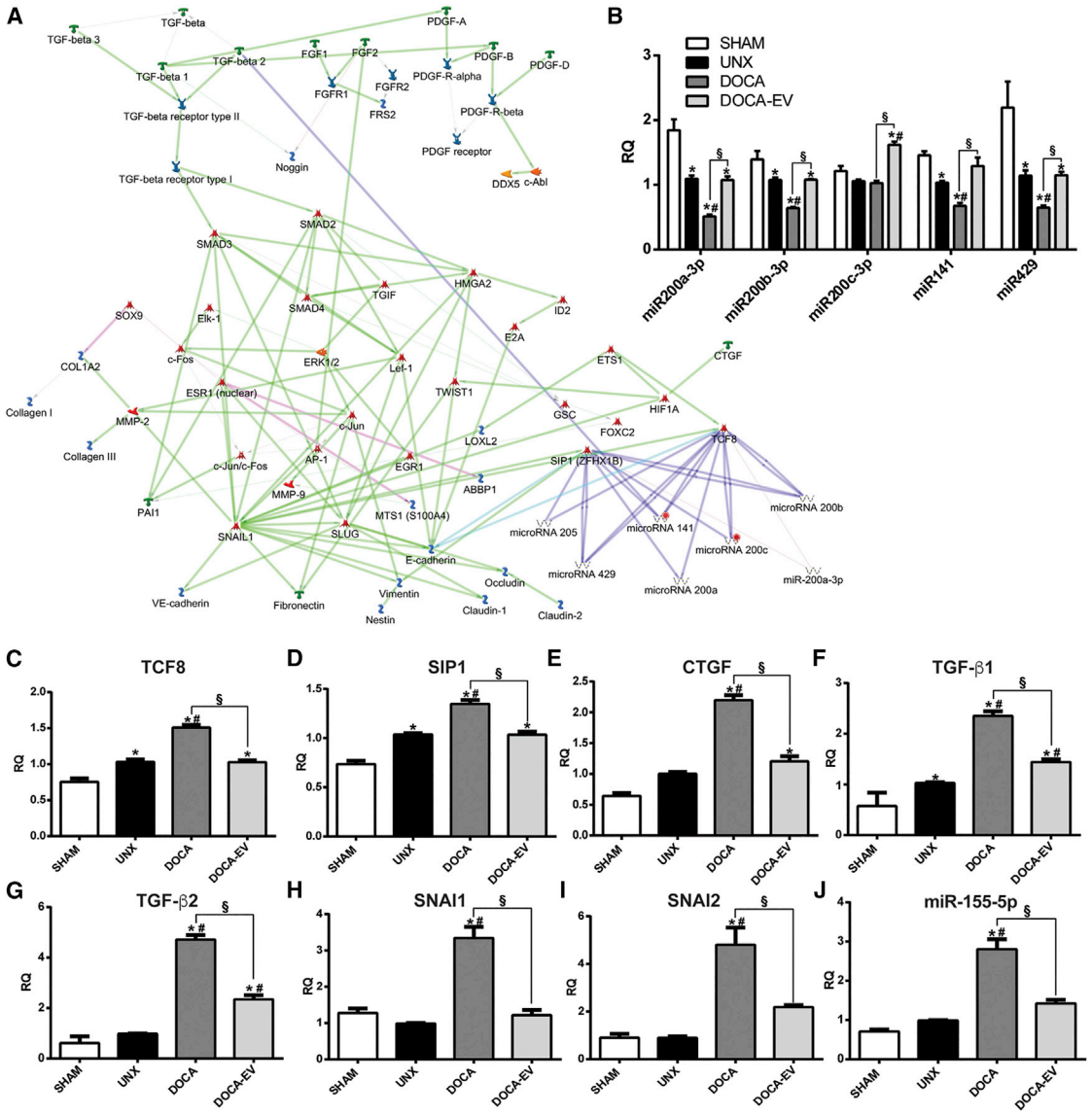

Figure 8. ASC-EVs Modulated miRNAs Associated with TGF-β-Dependent EMT and Fibrosis

(A) EMT pathway network generated by the overrepresented target-miRNA interactions built from the list of miRNAs modulated in UNX and DOCA-EV compared to DOCA rats. (B) Validation by quantitative real-time PCR of the expression of miR-200 family members in SHAM (n = 3) and in all the uninephrectomized animals (UNX, DOCA, and DOCA-EV, n = 6). (C–I) Analysis of the mRNA expression levels of the direct nodes of the miR-200 family *TCF8* (C) and *SIP1* (D), and the pro-fibrotic genes *CTGF* (E), *TGF-β1* (F), *TGF-β2* (G), *SNAI1* (H), and *SNAI2* (I) in the cortical tissue from SHAM (n = 3) and in all the uninephrectomized animal groups (UNX, n = 6; DOCA and DOCA-EV, n = 7). (J) miR-155-5p expression levels in the kidney from SHAM (n = 3) and in all the uninephrectomized animal groups (UNX, DOCA, and DOCA-EV, n = 6). Quantitative real-time PCR data were expressed as RQ and UNX was used as the reference sample. Data represent mean ± SE. *indicates statistical difference to UNX group, # indicates statistical difference to UNX group, and § indicates statistical difference to DOCA-EV group; $p < 0.05$.

complex and multitarget disease, dissecting the effect of EV administration on kidney-heart co-morbidity in the context of hypertension. We found that the beneficial effects of EVs covered multiple tissue/organs and could be ascribed to some a vascular protection mechanism, together with a tissue-protecting effect at both renal and heart levels. In our DOCA model, multiple administrations of ASC-EVs could in the first instance control the rise in the SBP, thus preventing any further increase from week 5 until sacrifice. Although it is difficult to dissect out the precise mechanism involved in the amelioration of SBP in EV-treated rats, we have speculated that ASC-EVs directly counterbalance hypertension by protecting the vasculature. This result is consistent with the effect reported for MSC-EV intravenous (i.v.) administration on the amelioration of pulmonary pressure and right ventricular pressure in a model of pulmonary hypertension.[37]

Interestingly, the ability of MSCs to beneficially regulate SBP has been previously associated with reduction of sympathetic activity affecting the cardiovascular system in a neurological model of hypertension.[38] Such modulation also resulted in the improvement of the renal architecture and microvascular rarefaction in the MSC-treated animals, suggesting that the regulation of SBP by ASC-EVs depends not only on a vascular effect but on a nervous system regulatory component.[38] In addition, 8-week-DOCA-treated animals had kidney and heart hypertrophy, indicating renal vasodilatation and cardiac overgrowth as a response to the high Na^+ load. Their excess weight was significantly reduced by EV treatment, suggesting the promotion of positive compensatory effects at tissue levels.

In concomitance with hemodynamic regulation, EV treatment promoted other beneficial effects to tissues, associated perhaps with anti-fibrotic mechanisms. ASC-EV administration reduced kidney damage, indicated by the decline of the renal injury score and *KIM-1* and *NGAL* expression. These markers associated with renal tubular injury were upregulated by DOCA treatment. KIM-1 is a cell-surface receptor that is upregulated in AKI and CKD. Increase in KIM-1 expression in CKD is associated with maladaptive response of renal tissue, stimulating inflammation and fibrosis.[39] NGAL is another important marker and a strong predictor of unfavorable renal outcomes and progression in CKD,[40] being directly correlated with declining renal function.[41] Reduction of both markers after ASC-EV administration underlines their protective effects on tubular processes. In addition, the protective effect of ASC-EVs was accompanied by reduction in renal accumulation of the marker of podocyte damage, Desmin,[42] and of the glomerular lesions observed in DOCA rats. All the protective effects of ASC-EVs on different nephron structures resulted in maintenance of kidney function at the same levels as uninephrectomy animals, indicated by our measurements of plasma creatine levels, normalized creatinine clearance, and proteinuria. The tissue-protecting effect of EVs was confirmed on different aspects of the profibrotic mechanisms, including renal apoptosis, increased cell proliferation, inflammation, collagen, and α-SMA accumulation, resulting in a "global" amelioration of kidney functions.

ASC-EVs induced a strong immunomodulatory response that inhibited macrophage recruitment (CD68 positive cells) to the kidney. This effect on macrophage accumulation may depend on EV-induced downregulation of *PAI1* and *MCP-1*, which are both upregulated in DOCA-salt rats. PAI1, a glycoprotein produced by resident and inflammatory cells, has a pro-fibrotic role and triggers a vicious cycle based on the recruitment of other inflammatory cells and fibroblast activation.[43] MCP-1 together with IL-6, also upregulated by DOCA treatment and reduced by EV administration, are multifunctional microinflammatory cytokines involved in immunoreaction and inflammation in hypertensive kidney disease.[44] Moreover, IL-6 is commonly found at high levels in the plasma of CKD patients[45] and has been associated with CKD progression through a mechanism involving promotion of renal injury and induction of chronic vascular disease.[46] Interestingly, recent reports highlighted the hypertensive state in DOCA-salt mice as an inflammation progress, where the inflammasome deficiency induces a fall in high BP, along with reduction of macrophages and pro-inflammatory cytokines in the kidneys compared to controls.[47] Chronic inflammation is not exclusive of HTN, but of other disorders, such as cardiovascular diseases.[48] Of note, in our model the beneficial immunomodulatory effects of the EV treatment were also seen in cardiac tissue, which had reduced fibrosis and macrophage infiltration compared to untreated DOCA-salt animals.

In order to understand the mechanisms associated with the therapeutic effects of ASC-EVs, we focused on the analysis of the miRNA signature in the renal tissue. Tissue and circulating miRNAs have recently emerged as mediators of intercellular communication and as potential biomarkers of cardiovascular and renal diseases.[49,50] Kidneys from DOCA-salt rats have a specific signature in which the most representative node was "development and regulation of EMT." The miR-200 family (miR-200a-3p, -200b-3p, -200c-3p, -141, and -429) includes well-known factors in the regulation of the EMT process.[51] Recent studies showed that 3 members of the miR-200 family (miR-200a-3p, miR-200b-3p, and miR-141) were markedly downregulated in ureteral obstruction (UUO) kidneys,[52] supporting their role in protecting tubular epithelial cells from dedifferentiation and EMT. We found that several members of the miR-200 family (miR-200a-3p, -200b-3p, -141, and -429) were downregulated by DOCA-salt treatment, and their expression reversed by EV administration. Importantly, we also found that the expression of several miR-200 family targets associated with the kidney fibrosis process was significantly inhibited by ASC-EVs (*SNAI1*, *SNAI2*, *TCF8*, *CTGF*, and *SIP1*). Of note, miR-200a-3p and -141 seem to impair progression of TGF-β-dependent EMT and fibrosis *in vitro* by direct downregulation of TGF-β2 expression.[53] In addition, the regulatory effects of miR-200b-3p were confirmed by i.v. administration of its synthetic precursor in UUO mice, thereby inhibiting the synthesis of FN, collagen types I and III, and reducing renal tubulointerstitial fibrosis.[54] Interestingly, our data suggest that this mechanism modulates the fibrotic process in DOCA-salt animals and that it represents a specific target of the ASC-EV treatment, in which the molecular content of EVs (proteins and RNAs) can activate an epigenetic modification able to directly modify the EMT and fibrosis pathways through the regulation of the axis miR-200-TGF-β.

Because DOCA-salt mimics a multi-organ chronic disease, the definition of the first organs targeted by EVs after their injection and what their immediate actions are could not be completely elucidated. Studies evaluating the effect of MSC-EVs after a short time from EV administration in AKI models have shown that EVs can promote the reduction of cell death and oxidative stress response in renal endothelial and epithelial cells.[55,56] Further biodistribution studies are necessary to encrypt these questions in chronic pathologies, such as CRS, in which the organs affected by the damage are more than one and targeted at different times. Moreover, our data sustained the use of EVs as a pharmacological drug, supporting a life treatment option for the patient affected by renal hypertension. Recently Braun

et al.[57] showed that multiple injections of MSC-derived exosomes in a model of neonatal chronic bronchopulmonary dysplasia were able to protect lung and heart from hyperoxia, preserving alveolar growth and inhibiting right heart hypertrophy. Intriguingly, these data support the capability of EVs to prompt a beneficial effect, after that the damage occurred independently from the first cause (hyperoxia) and also without a continuation of the treatment.[55] It is important to mention that in our protocol, the administration of ASC-EVs was maintained until the end of the treatment. Future experiments ceasing the administration of the EVs could give further information about the lasting EV effects in CKD models.

In conclusion, our results show that ASC-EVs administered in multiple doses can be effective as a therapy for the treatment of HTN and CRS, preventing CKD. Moreover, our findings indicate that miRNAs, in particular those of the miR-200 family, play a central role in CKD progression and evolution toward CRS, representing a therapeutic option in hypertensive-induced CKD.

MATERIALS AND METHODS

Cell Culture

Human ASCs were purchased from Lonza (Basel, Switzerland) and cultured in Adipose-Derived Stem Cell Growth BulletKit Medium (Lonza) at 37°C in a humidified atmosphere containing 5% CO_2 in air. Expression of classical ASCs surface markers allophycocyanin (APC), phycoerythrin (PE), and fluorescein (FITC) isothiocyanate-conjugated (CD44, CD90, CD73, CD105, all from BD Bioscience, San Jose, CA, USA) were confirmed by flow cytometry analysis (data not shown). As control, mouse isotypic immunoglobulin G (IgG) conjugated antibodies were used (BD Bioscience).

Extracellular Vesicles Isolation and Characterization

Briefly, when the ASCs reached ~70% confluency, they were washed twice with PBS and cultured in serum-free RPMI medium (Thermo Fisher Scientific, Waltham, MA, USA) for 72 h at 37°C in 5% CO_2 in air atmosphere. The conditioned medium was collected and centrifuged first at 2,000 × *g* for 20 min to remove debris and apoptotic bodies. Subsequently, EVs were purified by a 2 h ultracentrifugation at 100,000 × *g* at 4°C (Optima L-90K ultracentrifuge; Beckman Coulter, Brea, CA, USA). The resulting EVs pellet was resuspended in RPMI containing 1% DMSO (Sigma-Aldrich, St. Louis, MO, USA) and stored at −80°C. EVs were characterized for size distribution and quantified by NTA using ZetaView (Particle Metrix GmbH, Inning am Ammersee, Germany). The quantification of each preparation of EVs (n = 10) was repeated three times.

Qualitative analysis of EV surface markers was conducted by flow cytometry using a FACSCalibur instrument and CellQuest software (Becton Dickinson Bioscience PharMingen, Franklin Lake, NJ, USA). Because EVs are too small for FACSCalibur analysis, we bound EVs to latex beads (Aldehyde/Sulfate Latex Beads, 4% w/v, Thermo Fisher Scientific). Briefly, EVs (about 3×10^9) were co-incubated with 5 μL beads for 15 min at room temperature and for 45 min at 4°C in a final volume of 100 μL of PBS at pH 7.2, with 0.5% w/v lyophilized powder BSA (Sigma-Aldrich). After incubation, the EVs-beads solution was washed for 5 min by centrifugation at 2,000 × *g* to eliminate unbounded EVs.

EVs adsorbed to the beads were divided in different tubes and incubated for 45 min at 4°C with the following primary antibodies (all from Santa Cruz, Dallas, TX, USA): CD63 (1:20, sc-5275), CD9 (1:20, sc-13118), and CD81 (1:50, sc-31234). The EVs-beads solution was washed to remove unbounded antibodies. Anti-mouse PE and anti-goat FITC (A-11003 and A-11055, respectively; Thermo Fisher Scientific) secondary fluorescence antibodies (1: 500) were added to the tubes and incubated for 20 min at 4°C. The adsorbed EVs were washed and analyzed by flow cytometry. The EVs-beads solution incubated with secondary antibodies alone was used as negative control for analysis. The same analysis was conducted with ASCs, previously permeabilized for 15 min with a solution of 0.1% Triton (v/v) in PBS. The cells were labeled with the primary antibodies (1:100) and secondary antibodies (1:1,000) following standard labeling procedures.[58]

Transmission Electron Microscopy

TEM of cells and EVs were carried out as previously described.[58] Briefly, ASCs were washed in PBS (pH 7.2) fixed in 2.5% (w/v) glutaraldehyde with 4% (w/v) freshly prepared formaldehyde in 0.1 M cacodylate buffer (pH 7.2) for 24 h and post-fixed in 1% OsO_4 (w/v) plus 0.8% $K_4Fe(CN)_6$ (w/v) in 0.1 M cacodylate buffer for 40 min, dehydrated in acetone, and embedded in epoxide resin for electron microscopy analysis. ASC-EVs were adhered onto glow-discharged formvar-coated copper grids 300 mesh (EMS, Hartfield, PA, USA) for 10 min. Grids were subsequently negatively stained with 1% (w/v) aurothioglucose (USP, Sigma-Aldrich) in water for 30 s, dried with filter paper, and examined in an electron microscope operating at 120 kV (Tecnai Spirit microscope, Thermo Fisher Scientific).

DOCA-Salt Model

Animal studies were run in accordance with the Brazilian College of Animal guidelines, with all procedures receiving approval from the Institutional Committee for Animal Care and Use of the Federal University of Rio de Janeiro (CEUA, certificate 038/15 and A02/16-61-15). The DOCA-salt model was generated by a modified protocol from.[59] 7-week-old male Wistar rats were obtained from the animal facility of Biomedical Science Institute, University of São Paulo (São Paulo, Brazil).

After 1 week of acclimatization, animals were anesthetized by intraperitoneal injection of xylazine (5 mg/kg; Bayer S.A., São Paulo, Brazil) and ketamine (50 mg/kg; Cristália, Itapira, Brazil) and underwent unilateral nephrectomy (left kidney). 1 week later, the nephrectomized animals were randomly divided into 3 cohorts: (1) the normal salt control-group, which received standard-Na^+ diet chow (0.50% w/w Na^+, Rhoster Industria e Comercio, Araçoiaba da Serra, Brazil), and was injected subcutaneously with vehicle (soybean oil, 0.1 mL/animal) and weekly i.v. injection of vehicle, starting from week 2 after nephrectomy (100 μL of PBS plus DMSO

0.2 mg/week/~300 gr) (UNX, n = 10; one animal died during the treatment, animal tested n = 9); (2) the high-salt group, which received high-Na^+ diet (1.5% w/w Na^+, Rhoster) in combination with a subcutaneous administration of DOCA (D7000-5G, Sigma-Aldrich) (8 mg/kg, twice a week in soybean oil) and weekly i.v. injection of vehicle, starting from week 2 after nephrectomy (100 μL of PBS plus DMSO 0.2 mg/week/~300 gr) (DOCA, n = 16; three animals died during the treatment, animal tested n = 13); and (3) the high-salt group that received high-Na^+ diet in combination with a subcutaneous administration of deoxycorticosterone acetate, and weekly i.v. injection of ASC-EVs, starting from week 2 after nephrectomy (1.5×10^9/week in PBS plus DMSO 0.2 mg/week/~300 gr) (DOCA-EV, n = 10). A 4^{th} group of Sham-operated rats receiving standard-Na^+ diet was added as control (SHAM, n = 8). Animals were kept in a 12 h light/dark cycle under controlled temperature (22°C–24°C) and humidity (40%–60%), with free access to filtered water and respective diet *ad libitum* for 8 weeks after nephrectomy until sacrifice (from 9 to 17 weeks of age) (Figure 1).

Non-invasive Blood Pressure, Water Intake, and Urine Output Measurements

SBP and DBP were measured by the tail-cuff method (EFF306, Insight Instruments, Ribeirão Preto, Brazil), which allows repeated and reliable determinations to be made over a short period in conscious animals. The animals were kept at 30°C ± 2°C for 20 min. After stabilization, blood pressure of each rat was registered by performing 3 consecutive measurements and the final value considered was the average of these 3 measures. The measurements were conducted each 1 minute and the animals were run one by one. Blood pressure was recorded at the same time every week. Animal weight was also recorded for all the experiments until sacrifice.

Before the surgical procedure (time 0) and on weeks 3, 5, 7, and 9 after uninephrectomy, rats were individually housed in metabolic cages provided with water (200 mL/day) and regular or high-salt chow (25 g/day). In order to reduce physiologic changes induced by environment modification, the animals were acclimated in metabolic cages for 24 h before sample collection.[60] Urine output and water intake were measured within the following 24 h. In addition, a urine sample was collected and clarified by centrifugation ($600 \times g$ for 5 min) for biochemical analysis. At the time of sacrifice, blood samples (~6 mL) were collected in tubes previously rinsed with 1 mM Na_2EDTA and plasma was collected by centrifugation ($2000 \times g$ for 10 min). Plasma and urine samples were stored in aliquots at −20°C. The heart and the kidney were removed, their wet weights were recorded, and then they were processed for histological and molecular analysis.

Biochemical Analysis

Creatinine concentrations were measured in urine and plasma samples by the Jaffe's reaction method (K016, Bioclin, Belo Horizonte, Brazil).[61] Urinary protein excretion was determined by a colorimetric assay using a commercial kit (498, Proteinúria-PP, Gold Analisa, Belo Horizonte, Brazil) and measured as 24 h-protein urinary excretion (mg/24 h). Microalbuminuria was measured by immune turbidimetric assay (K078, Microalbuminuria, Bioclin). Na^+ and K^+ concentrations were measured by flame photometry (Analyzer, São Paulo, Brazil) in urine samples, as previous described.[62] Creatinine clearance[63] (CrC, normalized by body weight), urinary protein/urinary creatinine (concentration of proteins in the urine in respect to the concentration of urinary creatinine, mg/g, UP:Cr), and urinary albumin/urinary creatinine (concentration of albumin in the urine in respect to the concentration of urinary creatinine, mg/g, UA:Cr) were then calculated.

Tissue Histology and Immunohistochemical Analyses

The kidneys and hearts were fixed, dehydrated, and embedded in paraffin as previously described.[64] Heart slices (7-mm thick) were stained with Masson's trichrome for connective tissue accumulation. Fibrotic areas were assessed by Picrosirius red staining in both kidney and heart specimens to evaluate collagen deposition.

Macrophage/monocytes (CD68), PCNA, and the pre-fibrotic marker α-SMA were detected by immunohistochemistry using the following mouse monoclonal antibodies on 5 μm-thick paraffin sections: CD68, MCA341R (1:50, Bio-Rad, Hercules, CA, USA); PCNA, M0879 (1:100, Agilent Technologies); and α-SMA, ab7817 (1:50, Abcam, Cambridge, UK). Sections were submitted to heat-induced antigen retrieval by microwave heating at boiling point in 0.01 M Na-citrate buffer (pH 6.0). For CD68 staining, pre-incubation with 0.1% (w/v) trypsin solution was added to the protocol. Slides were incubated overnight in a humid chamber (4°C) with the primary antibodies, and binding was detected by incubation with Nichirei Histofine Rat Simple Stain anti-mouse secondary antibody (414171F, Tokyo, Japan) for 1 h at room temperature. Peroxidase activity was detected with 3,3′-diaminobenzidine (K3468 DAB, Agilent Technologies) as chromogen, and the slides were counterstained with hematoxylin. Negative controls consisted of sections incubated with an isotype-specific IgG were added.

The density of CD68 expression in the kidney and heart are given as a percentage of CD68 immunodetected and expressed as mean ± SEM. PCNA was determined by the number of positive cells/fields in the cortical and medullary regions of the kidney. Images were obtained using an Olympus AX70 microscope (Olympus, Japan), and the analysis was conducted using the ImageJ software (NIH, Bethesda, MD, USA) in at least 12 randomly captured photomicrographs.

Histological Score of Kidney Lesions

Kidney sections were examined by a pathologist in a blinded manner. Paraffin sections were stained with H&E and periodic acid-Schiff (PAS) and observed under light microscopy for qualitative and quantitative analysis. Tubulointerstitial injury was scored based on the following tubule alterations: loss/disruption of brush border in proximal tubule cells, cellular vacuolization in all nephron segments, cell death with detachment from basement membrane culminating in tubular cell desquamation, tubular dilation due to tubular obstruction, casts accumulation in the tubular space, and later, tubular

atrophy due to the loss of viable tubular cells. Glomerular lesions were scored after the observation of 100 glomeruli (transverse sections) from each animal in PAS stained sections. Glomerular injury consisted of capsular thickening, mesangial axis enlargement, and the presence of glomerulosclerosis (segmental or global). Vascular damage was characterized by the luminal diminution, myointimal hyperplasia, hyaline arteriopathy, and fibrinoid necrosis.

Semiquantitative data were obtained from high-quality photomicrographs (2,048 × 1,536 pixel buffer) using a digital camera (Evolution VF, Media Cybernetics, Bethesda, MD, USA) connected to Nikon Eclipse E-800 light microscope and the graphical interface software Q-capture 2.95.0, version 2.0.5 (Silicon Graphic, Milpitas, CA, USA). Ten non-overlapping images of vessels (arteriole and artery), or tubules (kidney cortex, and outer medulla), were randomly obtained with a 40× (tubular profiles) or a 20× (glomerular and vascular profiles) objective lens from each kidney section stained with PAS (tubular profiles), or H&E (vascular profiles) (animals/group: SHAM, n = 4; UNX, n = 9; DOCA, n = 13; DOCA-EV, n = 10). Histological lesions were graded from 0−3 as follows: 0, absence; 0.5, up to 10% injured tubules, glomeruli, vessels, or interstitial area; 1.0, 11%−25%; 1.5, 26%−45%; 2.0, 46%−60%; 2.5, 61%−75%; 3.0, ≥76%. A histological injury score was produced for each profile (tubular, vascular, or glomerular) and was obtained by the sum of all the values of the respective damage parameters analyzed.[17]

Western Blotting

Kidney cortex extracts were homogenized in radioimmunoprecipitation assay (RIPA) buffer supplemented with protease and phosphatase inhibitor cocktail and PMSF (Sigma-Aldrich). Protein content was determined by the Folin-phenol method,[65] using BSA as a standard. Aliquots of 30 μg proteins were run on 10%–12% SDS-PAGE under reducing conditions, and western blotting was carried out as previously described.[65] The following primary antibodies were used: GAPDH, sc-32233 (1:1,000, Santa Cruz); α-SMA, MAB1420 (1:1,000, R&D Systems, Minneapolis, MN, USA); Desmin, ab32362 (1:1,000, Abcam); B cell lymphoma 2 (Bcl2), 2876 (1:1,000, Cell Signaling Technology, Danvers, MA, USA); and Bcl-2-associated X (Bax), 2772S (1:500, Cell Signaling Technology). The secondary antibodies were anti-rabbit and anti-mouse IgG-horseradish peroxidase (HRP) (NA934-1 and NA931, 1:5,000 and 1:10,000, GE Healthcare, Buckinghamshire, UK). Proteins were detected by chemiluminescence using the ECL system (GE Healthcare) and ChemiDoc XRS+ (Bio-Rad). Quantification of western blots was performed with ImageJ software (NIH).

Microarrays Profile and Quantitative Real-Time PCR

The Absolutely RNA miRNA Kit (400814, Agilent Technologies) was used for RNA extraction from renal tissue. The yield of the extracted RNA was determined spectrophotometrically (Nanodrop-1000, Thermo Scientific). RNA integrity and quality were evaluated using RNA 6000 Nano Chip and Agilent 2100 Bioanalyzer (Agilent Technologies). RNA samples with RNA integrity numbers (RINs) > 8.0 were used for microarray experiments.[66]

Single color (Cy3) miRNA Array (8 × 15k) (for the screening of 780 mature miRNAs) and reagents were used (Agilent Technologies) using 100 ng of total RNA for the labeling and hybridization procedures. Microarray profile analysis was conducted on a pool of 4 animals/treatment (SHAM, UNX, DOCA, and DOCA-EV) and were repeated using different experimental groups. An Agilent one-color spike in kit was used as a positive control to measure both the labeling and hybridization procedures. Data were analyzed using the Agilent GeneSpring GX Data software (Agilent Technologies), where the expressed miRNAs were defined as entities detected in at least 80% of the values of any of the 4 conditions. Microarray data have been deposited in the GEO "GEO: GSE139660". Differential expression was determined by a fold change ≥1.5 to define upregulation or downregulation with respect to DOCA-salt treatment. A pathway enrichment analysis used MetaCore software v.6.35 (Thomson Reuters, Toronto, Canada). A Venn diagram was generated using the online software of Bioinformatics & Evolutionary Genomics.[67]

Microarrays data were confirmed by quantitative real-time PCR, using the miRNA 1st Strand Synthesis and miRNA qPCR Master Mix kits (both from Agilent Technologies). Negative non-polyadenylated RNA controls and negative cDNA controls (no cDNA) were cycled to the specificity of the detection. Mature Let-7a was used as miRNA internal reference after stability and expression test on a panel of representative samples. mRNA data analysis used the High Capacity cDNA Reverse Transcription Kit and the Power SYBR Green PCR Master Mix (from Life Technologies) in a ViiA 7 Real-Time PCR System (Life Technologies). The run conditions were as follows: 95°C for 10 min, followed by 40 cycles of 30 s at 95°C and 1 min at 60°C. Melting curve analysis was added to the run. The sequence-specific oligonucleotide primers were all obtained from Eurofins Genomics (Eurofins Brazil, Indaiatuba, Brazil). Negative cDNA controls (no cDNA) were cycled in parallel with each run. GAPDH was used as the mRNA internal reference, and the fold expression was calculated according to the $2^{-\Delta\Delta Ct}$ method,[68] using the UNX as reference sample (UNX = 1). The primers used in quantitative real-time PCR experiments are described in Table S3.

Statistical Analysis

Where appropriate, results are expressed as mean ± SEM. Statistical analysis used one-way ANOVA followed by Tukey's multiple comparison test or t test where necessary. Differences were considered significant at $p < 0.05$.

SUPPLEMENTAL INFORMATION

Supplemental Information can be found online at https://doi.org/10.1016/j.omtm.2019.11.002.

AUTHOR CONTRIBUTIONS

Conceptualization: R.S.L., A. Vieyra, and F.C. Methodology: R.S.L., C.M.T., K.R.M., L.S.L., and F.C. Investigation: R.S.L., J.L., R.B., C.M.T., and F.C. Writing – Original Draft: R.S.L., A. Vieyra, and F.C. Writing –Review & Editing: R.S.L., B.B., A. Viola, A. Vieyra,

and F.C. Funding Acquisition: R.S.L., A. Vieyra, and F.C. Resources: C.M.T., K.R.M., and B.B. Supervision: E.A., L.S.L., and K.R.M.

CONFLICTS OF INTEREST

The authors declare no competing interests.

ACKNOWLEDGMENTS

The English style and presentation of this manuscript were corrected by BioMedES UK (https://www.biomedes.biz/), which is gratefully acknowledged. This work was supported by National Institute of Science and Technology for Regenerative Medicine REGENERA (grant number 465656/2014-5); the Brazilian National Research Council (grant numbers 421916/2016-8, 404092/2012-8, 457222/2013-1, 403151/2015-5, and 307605/2015-9); and the Carlos Filho Rio de Janeiro State Research Foundation (grant numbers E-26/201.142/2014 and E-26/010.001283/2015). We also acknowledge the access to the facilities at the National Center of Structural Biology and Bioimaging-CENABIO, Federal University of Rio de Janeiro.

REFERENCES

1. Mills, K.T., Chen, J., Yang, W., Appel, L.J., Kusek, J.W., Alper, A., Delafontaine, P., Keane, M.G., Mohler, E., Ojo, A., et al.; Chronic Renal Insufficiency Cohort (CRIC) Study Investigators (2016). Sodium Excretion and the Risk of Cardiovascular Disease in Patients With Chronic Kidney Disease. JAMA *315*, 2200–2210.
2. Tedla, F.M., Brar, A., Browne, R., and Brown, C. (2011). Hypertension in chronic kidney disease: navigating the evidence. Int. J. Hypertens. *2011*, 132405.
3. Carretero, O.A., and Oparil, S. (2000). Essential hypertension. Part I: definition and etiology. Circulation *101*, 329–335.
4. Fogo, A.B. (2007). Mechanisms of progression of chronic kidney disease. Pediatr. Nephrol. *22*, 2011–2022.
5. Borthwick, L.A., Wynn, T.A., and Fisher, A.J. (2013). Cytokine mediated tissue fibrosis. Biochim. Biophys. Acta *1832*, 1049–1060.
6. Benigni, A., Morigi, M., and Remuzzi, G. (2010). Kidney regeneration. Lancet *375*, 1310–1317.
7. González, A., Ravassa, S., López, B., Moreno, M.U., Beaumont, J., San José, G., Querejeta, R., Bayés-Genís, A., and Díez, J. (2018). Myocardial Remodeling in Hypertension. Hypertension *72*, 549–558.
8. Brunner, H.R., Laragh, J.H., Baer, L., Newton, M.A., Goodwin, F.T., Krakoff, L.R., Bard, R.H., and Bühler, F.R. (1972). Essential hypertension: renin and aldosterone, heart attack and stroke. N. Engl. J. Med. *286*, 441–449.
9. Cruz, D.N. (2013). Cardiorenal syndrome in critical care: the acute cardiorenal and renocardiac syndromes. Adv. Chronic Kidney Dis. *20*, 56–66.
10. McCullough, P.A., Kellum, J.A., Haase, M., Müller, C., Damman, K., Murray, P.T., Cruz, D., House, A.A., Schmidt-Ott, K.M., Vescovo, G., et al. (2013). Pathophysiology of the cardiorenal syndromes: executive summary from the eleventh consensus conference of the Acute Dialysis Quality Initiative (ADQI). Contrib. Nephrol *182*, 82–98.
11. Virzì, G., Day, S., de Cal, M., Vescovo, G., and Ronco, C. (2014). Heart-kidney cross-talk and role of humoral signaling in critical illness. Crit. Care *18*, 201–211.
12. Bongartz, L.G., Braam, B., Gaillard, C.A., Cramer, M.J., Goldschmeding, R., Verhaar, M.C., Doevendans, P.A., and Joles, J.A. (2012). Target organ cross talk in cardiorenal syndrome: animal models. Am. J. Physiol. Renal Physiol. *303*, F1253–F1263.
13. Basting, T., and Lazartigues, E. (2017). DOCA-Salt Hypertension: an Update. Curr. Hypertens. Rep. *19*, 32–46.
14. Fink, G.D., Johnson, R.J., and Galligan, J.J. (2000). Mechanisms of increased venous smooth muscle tone in desoxycorticosterone acetate-salt hypertension. Hypertension *35*, 464–469.
15. Dobrzynski, E., Wang, C., Chao, J., and Chao, L. (2000). Adrenomedullin gene delivery attenuates hypertension, cardiac remodeling, and renal injury in deoxycorticosterone acetate-salt hypertensive rats. Hypertension *36*, 995–1001.
16. Karatas, A., Hegner, B., de Windt, L.J., Luft, F.C., Schubert, C., Gross, V., Akashi, Y.J., Gürgen, D., Kintscher, U., da Costa Goncalves, A.C., et al. (2008). Deoxycorticosterone acetate-salt mice exhibit blood pressure-independent sexual dimorphism. Hypertension *51*, 1177–1183.
17. Bae, E.H., Kim, I.J., Park, J.W., Ma, S.K., Lee, J.U., and Kim, S.W. (2010). Renoprotective effect of rosuvastatin in DOCA-salt hypertensive rats. Nephrol. Dial. Transplant. *25*, 1051–1059.
18. Grange, C., Iampietro, C., and Bussolati, B. (2017). Stem cell extracellular vesicles and kidney injury. Stem Cell Investig. *4*, 90.
19. Bateman, M.E., Strong, A.L., Gimble, J.M., and Bunnell, B.A. (2018). Concise Review: Using Fat to Fight Disease: A Systematic Review of Nonhomologous Adipose-Derived Stromal/Stem Cell Therapies. Stem Cells *36*, 1311–1328.
20. Keshtkar, S., Azarpira, N., and Ghahremani, M.H. (2018). Mesenchymal stem cell-derived extracellular vesicles: novel frontiers in regenerative medicine. Stem Cell Res. Ther. *9*, 63–72.
21. Papazova, D.A., Oosterhuis, N.R., Gremmels, H., van Koppen, A., Joles, J.A., and Verhaar, M.C. (2015). Cell-based therapies for experimental chronic kidney disease: a systematic review and meta-analysis. Dis. Model. Mech. *8*, 281–293.
22. He, J., Wang, Y., Lu, X., Zhu, B., Pei, X., Wu, J., and Zhao, W. (2015). Micro-vesicles derived from bone marrow stem cells protect the kidney both in vivo and in vitro by microRNA-dependent repairing. Nephrology (Carlton) *20*, 591–600.
23. Jiang, Z.Z., Liu, Y.M., Niu, X., Yin, J.Y., Hu, B., Guo, S.C., Fan, Y., Wang, Y., and Wang, N.S. (2016). Exosomes secreted by human urine-derived stem cells could prevent kidney complications from type I diabetes in rats. Stem Cell Res. Ther. *7*, 24–35.
24. van Koppen, A., Joles, J.A., van Balkom, B.W., Lim, S.K., de Kleijn, D., Giles, R.H., and Verhaar, M.C. (2012). Human embryonic mesenchymal stem cell-derived conditioned medium rescues kidney function in rats with established chronic kidney disease. PLoS ONE *7*, e38746.
25. Binato, R., Santos, E.C., Boroni, M., Demachki, S., Assumpção, P., and Abdelhay, E. (2017). A common molecular signature of intestinal-type gastric carcinoma indicates processes related to gastric carcinogenesis. Oncotarget *9*, 7359–7371.
26. Rosivatz, E., Becker, I., Specht, K., Fricke, E., Luber, B., Busch, R., Höfler, H., and Becker, K.F. (2002). Differential expression of the epithelial-mesenchymal transition regulators snail, SIP1, and twist in gastric cancer. Am. J. Pathol. *161*, 1881–1891.
27. Sierra-Mondragon, E., Rodríguez-Muñoz, R., Namorado-Tonix, C., Molina-Jijon, E., Romero-Trejo, D., Pedraza-Chaverri, J., and Reyes, J.L. (2019). All-Trans Retinoic Acid Attenuates Fibrotic Processes by Downregulating TGF-β1/Smad3 in Early Diabetic Nephropathy. Biomolecules *9*, E525.
28. Saucedo, A.L., Perales-Quintana, M.M., Paniagua-Vega, D., Sanchez-Martinez, C., Cordero-Perez, P., and Minsky, N.W. (2018). Chronic Kidney Disease and the Search for New Biomarkers for Early Diagnosis. Curr. Med. Chem. *25*, 3719–3747.
29. Kandlikar, S.S., and Fink, G.D. (2011). Mild DOCA-salt hypertension: sympathetic system and role of renal nerves. Am. J. Physiol. Heart Circ. Physiol. *300*, H1781–H1787.
30. Titze, J., Bauer, K., Schafflhuber, M., Dietsch, P., Lang, R., Schwind, K.H., Luft, F.C., Eckardt, K.U., and Hilgers, K.F. (2005). Internal sodium balance in DOCA-salt rats: a body composition study. Am. J. Physiol. Renal Physiol. *289*, F793–F802.
31. Iliescu, R., Fernandez, S.R., Kelsen, S., Maric, C., and Chade, A.R. (2010). Role of renal microcirculation in experimental renovascular disease. Nephrol. Dial. Transplant. *25*, 1079–1087.
32. Gu, J.W., Bailey, A.P., Tan, W., Shparago, M., and Young, E. (2008). Long-term High Salt Diet Causes Hypertension and Decreases Renal Expression of Vascular Endothelial Growth Factor in Sprague-Dawley Rats. J. Am. Soc. Hypertens. *2*, 275–285.
33. Bae, E.H., Kim, I.J., Song, J.H., Choi, H.S., Kim, C.S., Eom, G.H., Kim, I., Cha, H., Cho, J.M., Ma, S.K., and Kim, S.W. (2019). Renoprotective Effect of the Histone Deacetylase Inhibitor CG200745 in DOCA-Salt Hypertensive Rats. Int. J. Mol. Sci. *20*, 508–521.

34. Gatti, S., Bruno, S., Deregibus, M.C., Sordi, A., Cantaluppi, V., Tetta, C., and Camussi, G. (2011). Microvesicles derived from human adult mesenchymal stem cells protect against ischaemia-reperfusion-induced acute and chronic kidney injury. Nephrol. Dial. Transplant. *26*, 1474–1483.

35. Eirin, A., Zhu, X.Y., Puranik, A.S., Tang, H., McGurren, K.A., van Wijnen, A.J., Lerman, A., and Lerman, L.O. (2017). Mesenchymal stem cell-derived extracellular vesicles attenuate kidney inflammation. Kidney Int. *92*, 114–124.

36. Kholia, S., Herrera Sanchez, M.B., Cedrino, M., Papadimitriou, E., Tapparo, M., Deregibus, M.C., Brizzi, M.F., Tetta, C., and Camussi, G. (2018). Human Liver Stem Cell-Derived Extracellular Vesicles Prevent Aristolochic Acid-Induced Kidney Fibrosis. Front. Immunol. *9*, 1639–1655.

37. Chen, J.Y., An, R., Liu, Z.J., Wang, J.J., Chen, S.Z., Hong, M.M., Liu, J.H., Xiao, M.Y., and Chen, Y.F. (2014). Therapeutic effects of mesenchymal stem cell-derived microvesicles on pulmonary arterial hypertension in rats. Acta Pharmacol. Sin. *35*, 1121–1128.

38. Oliveira-Sales, E.B., Maquigussa, E., Semedo, P., Pereira, L.G., Ferreira, V.M., Câmara, N.O., Bergamaschi, C.T., Campos, R.R., and Boim, M.A. (2013). Mesenchymal stem cells (MSC) prevented the progression of renovascular hypertension, improved renal function and architecture. PLoS ONE *8*, e78464.

39. Humphreys, B.D., Xu, F., Sabbisetti, V., Grgic, I., Movahedi Naini, S., Wang, N., Chen, G., Xiao, S., Patel, D., Henderson, J.M., et al. (2013). Chronic epithelial kidney injury molecule-1 expression causes murine kidney fibrosis. J. Clin. Invest. *123*, 4023–4035.

40. Castillo-Rodriguez, E., Fernandez-Prado, R., Martin-Cleary, C., Pizarro-Sánchez, M.S., Sanchez-Niño, M.D., Sanz, A.B., Fernandez-Fernandez, B., and Ortiz, A. (2017). Kidney Injury Marker 1 and Neutrophil Gelatinase-Associated Lipocalin in Chronic Kidney Disease. Nephron *136*, 263–267.

41. Bolignano, D., Coppolino, G., Lacquaniti, A., and Buemi, M. (2009). Neutrophil gelatinase-associated lipocalin in the intensive care unit: time to look beyond a single, threshold-based measurement? Crit. Care Med. *37*, 2864–2865, author reply 2864–2865.

42. Li, Y., Kang, Y.S., Dai, C., Kiss, L.P., Wen, X., and Liu, Y. (2008). Epithelial-to-mesenchymal transition is a potential pathway leading to podocyte dysfunction and proteinuria. Am. J. Pathol. *172*, 299–308.

43. Eddy, A.A., and Fogo, A.B. (2006). Plasminogen activator inhibitor-1 in chronic kidney disease: evidence and mechanisms of action. J. Am. Soc. Nephrol. *17*, 2999–3012.

44. Xue, H.Y., Yuan, L., Cao, Y.J., Fan, Y.P., Chen, X.L., and Huang, X.Z. (2016). Resveratrol ameliorates renal injury in spontaneously hypertensive rats by inhibiting renal micro-inflammation. Biosci. Rep. *36*, e00339–e00350.

45. Amdur, R.L., Feldman, H.I., Dominic, E.A., Anderson, A.H., Beddhu, S., Rahman, M., Wolf, M., Reilly, M., Ojo, A., Townsend, R.R., et al.; CRIC Study Investigators (2019). Use of Measures of Inflammation and Kidney Function for Prediction of Atherosclerotic Vascular Disease Events and Death in Patients With CKD: Findings From the CRIC Study. Am. J. Kidney Dis. *73*, 344–353.

46. Agharazii, M., St-Louis, R., Gautier-Bastien, A., Ung, R.V., Mokas, S., Larivière, R., and Richard, D.E. (2015). Inflammatory cytokines and reactive oxygen species as mediators of chronic kidney disease-related vascular calcification. Am. J. Hypertens. *28*, 746–755.

47. Krishnan, S.M., Dowling, J.K., Ling, Y.H., Diep, H., Chan, C.T., Ferens, D., Kett, M.M., Pinar, A., Samuel, C.S., Vinh, A., et al. (2016). Inflammasome activity is essential for one kidney/deoxycorticosterone acetate/salt-induced hypertension in mice. Br. J. Pharmacol. *173*, 752–765.

48. Youn, J.C. (2016). Sy 17-3 role of cmv induced T cell senescence in the pathophysiology of cardiovascular disease. J Hypertens *34*, e535, Suppl 1- ISH 2016 Abstract Book.

49. Creemers, E.E., Tijsen, A.J., and Pinto, Y.M. (2012). Circulating microRNAs: novel biomarkers and extracellular communicators in cardiovascular disease? Circ. Res. *110*, 483–495.

50. Muralidharan, J., Ramezani, A., Hubal, M., Knoblach, S., Shrivastav, S., Karandish, S., Scott, R., Maxwell, N., Ozturk, S., Beddhu, S., et al. (2017). Extracellular microRNA signature in chronic kidney disease. Am. J. Physiol. Renal Physiol. *312*, F982–F991.

51. Xiong, M., Jiang, L., Zhou, Y., Qiu, W., Fang, L., Tan, R., Wen, P., and Yang, J. (2012). The miR-200 family regulates TGF-β1-induced renal tubular epithelial to mesenchymal transition through Smad pathway by targeting ZEB1 and ZEB2 expression. Am. J. Physiol. Renal Physiol. *302*, F369–F379.

52. Chung, A.C., Huang, X.R., Meng, X., and Lan, H.Y. (2010). miR-192 mediates TGF-beta/Smad3-driven renal fibrosis. J. Am. Soc. Nephrol. *21*, 1317–1325.

53. Wang, B., Koh, P., Winbanks, C., Coughlan, M.T., McClelland, A., Watson, A., Jandeleit-Dahm, K., Burns, W.C., Thomas, M.C., Cooper, M.E., and Kantharidis, P. (2011). miR-200a Prevents renal fibrogenesis through repression of TGF-β2 expression. Diabetes *60*, 280–287.

54. Oba, S., Kumano, S., Suzuki, E., Nishimatsu, H., Takahashi, M., Takamori, H., Kasuya, M., Ogawa, Y., Sato, K., Kimura, K., et al. (2010). miR-200b precursor can ameliorate renal tubulointerstitial fibrosis. PLoS ONE *5*, e13614–e13620.

55. Zhang, G., Zou, X., Miao, S., Chen, J., Du, T., Zhong, L., Ju, G., Liu, G., and Zhu, Y. (2014). The anti-oxidative role of micro-vesicles derived from human Wharton-Jelly mesenchymal stromal cells through NOX2/gp91(phox) suppression in alleviating renal ischemia-reperfusion injury in rats. PLoS ONE *9*, e92129.

56. Zhang, G., Zou, X., Huang, Y., Wang, F., Miao, S., Liu, G., Chen, M., and Zhu, Y. (2016). Mesenchymal Stromal Cell-Derived Extracellular Vesicles Protect Against Acute Kidney Injury Through Anti-Oxidation by Enhancing Nrf2/ARE Activation in Rats. Kidney Blood Press. Res. *41*, 119–128.

57. Braun, R.K., Chetty, C., Balasubramaniam, V., Centanni, R., Haraldsdottir, K., Hematti, P., and Eldridge, M.W. (2018). Intraperitoneal injection of MSC-derived exosomes prevent experimental bronchopulmonary dysplasia. Biochem. Biophys. Res. Commun. *503*, 2653–2658.

58. Collino, F., Lopes, J.A., Corrêa, S., Abdelhay, E., Takiya, C.M., Wendt, C.H.C., de Miranda, K.R., Vieyra, A., and Lindoso, R.S. (2019). Adipose-Derived Mesenchymal Stromal Cells Under Hypoxia: Changes in Extracellular Vesicles Secretion and Improvement of Renal Recovery after Ischemic Injury. Cell. Physiol. Biochem. *52*, 1463–1483.

59. Moreira, C.M., Meira, E.F., Vestena, L., Stefanon, I., Vassallo, D.V., and Padilha, A.S. (2012). Tension cost correlates with mechanical and biochemical parameters in different myocardial contractility conditions. Clinics (São Paulo) *67*, 489–496.

60. Gomes, P.M., Sá, R.W.M., Aguiar, G.L., Paes, M.H.S., Alzamora, A.C., Lima, W.G., de Oliveira, L.B., Stocker, S.D., Antunes, V.R., and Cardoso, L.M. (2017). Chronic high-sodium diet intake after weaning lead to neurogenic hypertension in adult Wistar rats. Sci. Rep. *7*, 5655–5669.

61. Slot, C. (1965). Plasma creatinine determination. A new and specific Jaffe reaction method. Scand. J. Clin. Lab. Invest. *17*, 381–387.

62. Cortes, A.L., Gonsalez, S.R., Rioja, L.S., Oliveira, S.S.C., Santos, A.L.S., Prieto, M.C., Melo, P.A., and Lara, L.S. (2018). Protective outcomes of low-dose doxycycline on renal function of Wistar rats subjected to acute ischemia/reperfusion injury. Biochim Biophys Acta Mol Basis Dis *1864*, 102–114.

63. Mima, A., Matsubara, T., Arai, H., Abe, H., Nagai, K., Kanamori, H., Sumi, E., Takahashi, T., Iehara, N., Fukatsu, A., et al. (2006). Angiotensin II-dependent Src and Smad1 signaling pathway is crucial for the development of diabetic nephropathy. Lab. Invest. *86*, 927–939.

64. Beiral, H.J., Rodrigues-Ferreira, C., Fernandes, A.M., Gonsalez, S.R., Mortari, N.C., Takiya, C.M., Sorenson, M.M., Figueiredo-Freitas, C., Galina, A., and Vieyra, A. (2014). The impact of stem cells on electron fluxes, proton translocation, and ATP synthesis in kidney mitochondria after ischemia/reperfusion. Cell Transplant. *23*, 207–220.

65. Luzardo, R., Silva, P.A., Einicker-Lamas, M., Ortiz-Costa, S., do Carmo, Mda.G., Vieira-Filho, L.D., Paixão, A.D., Lara, L.S., and Vieyra, A. (2011). Metabolic programming during lactation stimulates renal Na+ transport in the adult offspring due to an early impact on local angiotensin II pathways. PLoS ONE *6*, e21232.

66. Kwekel, J.C., Vijay, V., Desai, V.G., Moland, C.L., and Fuscoe, J.C. (2015). Age and sex differences in kidney microRNA expression during the life span of F344 rats. Biol. Sex Differ. *6*, 1–16.

67. VIB/UGent Bioinformatics & Evolutionary Genomics. Bioinformatics & Evolutionary Genomics. http://bioinformatics.psb.ugent.be/software/details/Venn-Diagrams.

68. Livak, K.J., and Schmittgen, T.D. (2001). Analysis of relative gene expression data using real-time quantitative PCR and the 2(-Delta Delta C(T)) Method. Methods *25*, 402–408.